ISSN 1674-1056
http://cpb.iphy.ac.cn
http://iopscience.iop.org/cpb
中国物理 B
Chinese Physics
中国物理 Chinese Physics B

Ultra-thin and light-weight spoof surface plasmon polariton coupler achieved by broadside coupled split ring resonators

Ya Fan(范亚), Jia-Fu Wang(王甲富), Hua Ma(马华), Yong-Feng Li(李勇峰), Ming-De Feng(冯明德), Shao-Bo Qu(屈绍波)
Citation: Chin. Phys. B . 2018, 27(10): 100304. **doi:** 10.1088/1674-1056/27/10/100304

Journal homepage: http://cpb.iphy.ac.cn; http://iopscience.iop.org/cpb

What follows is a list of articles you may be interested in

Observation of geometric phase in a dispersively coupled resonator-qutrit system

Libo Zhang(张礼博), Chao Song(宋超), H Wang(王浩华), Shi-Biao Zheng(郑仕标)

Chin. Phys. B . 2018, 27(7): 070303. **doi:** 10.1088/1674-1056/27/7/070303

Tunable two-axis spin model and spin squeezing in two cavities

Lixian Yu(俞立先), Caifeng Li(李彩凤), Jingtao Fan(樊景涛), Gang Chen(陈刚), Tian-Cai Zhang(张天才), Suotang Jia(贾锁堂)
Chin. Phys. B . 2016, 25(5): 050301. **doi:** 10.1088/1674-1056/25/5/050301

Ground-state information geometry and quantum criticality in an inhomogeneous spin model

Ma Yu-Quan
Chin. Phys. B . 2015, 24(9): 090301. **doi:** 10.1088/1674-1056/24/9/090301

Topological phase transitions driven by next-nearest-neighbor hopping in noncentrosymmetric cold Fermi gases

Wang Rui, Zhang Cun-Xi, Ji Qing-Shan
Chin. Phys. B . 2015, 24(3): 030305. **doi:** 10.1088/1674-1056/24/3/030305

Topological properties of one-dimensional hardcore Bose-Fermi mixture

Jia Yong-Fei, Guo Huai-Ming, Qin Ji-Hong, Chen Zi-Yu, Feng Shi-Ping
Chin. Phys. B . 2013, 22(9): 090308. **doi:** 10.1088/1674-1056/22/9/090308

Ultra-thin and light-weight spoof surface plasmon polariton coupler achieved by broadside coupled split ring resonators*

Ya Fan(范亚), Jia-Fu Wang(王甲富)†, Hua Ma(马华), Yong-Feng Li(李勇峰), Ming-De Feng(冯明德), and Shao-Bo Qu(屈绍波)‡

Department of Basic Sciences, Air Force Engineering University, Xi'an 710051, *China*

(Received 19 April 2018; revised manuscript received 4 June 2018; published online 10 September 2018)

Low profile and light weight are very important for practical applications of a spoof surface plasmon polariton (SSPP) coupler, especially at low frequencies. In this paper, we propose and design an ultra-thin, light-weight SSPP coupler based on broadside coupled split ring resonators (BC-SRRs). The size of BC-SRR can be far less than $\lambda/100$ and can extremely well control the reflective phases within a subwavelength thickness. Due to the broadside capacitive coupling, the electrical size of BC-SRR is dramatically reduced to guarantee the ultra-thin thickness of the SSPP coupler. The weight of the SSPP coupler is reduced by a low occupation ratio of BC-SRR in the unit cell volume. As an example, a C-band SSPP coupler composed of phase gradient BC-SRRs is designed, fabricated, and measured. Due to the ultra-small size and low occupation ratio of BC-SRRs, the thickness of the coupler is $\lambda/12$ and the surface density is only 0.98 kg/m^2. Both simulation and experiment results verify that the coupler can achieve high-efficiency SPP coupling at 5.27 GHz under normal incidence.

Keywords: ultra-thin, light-weight, poof surface plasmon polariton, broadside coupling

PACS: 03.65.Vf, 41.20.Jb, 81.05.Xj **DOI:** 10.1088/1674-1056/27/10/100304

1. Introduction

Surface plasmon polariton (SPP)[1–3] refers to a hybrid mode of electromagnetic waves and electron density oscillations bound to the interface, with exponentially decaying field intensity in the direction perpendicular to the interface. Owing to a dramatically compressed wavelength, SPPs exhibit many unique properties[4] and have been widely applied to chemical and bio-sensing,[5] plasmonic circuits and waveguides,[6] super-resolution imaging,[7] etc. To explore these excellent properties at far infrared, terahertz, and microwave frequencies, spoof surface plasmon polaritons (SSPPs)[8,9] are excited by bulky gratings or dielectric prisms, showing very similar electromagnetic behaviors to SPPs at optical frequencies. An alternative high-efficiency SSPP coupler has been proposed and demonstrated, which is composed of periodically arranged phase gradient split ring resonators (SRRs). The metallic structures are patterned on a planar solid dielectric substrate, so such couplers are also known as phase gradient metasurfaces[10–15] (PGMs). Different abrupt phase changes can be obtained by adjusting the geometric parameters of resonators. By designing the phase gradient on PGMs, a predefined parallel wave vector is formed to compensate for the wave-vector difference between free-space waves and SSPPs. Once this additional wave vector is larger than that in free space, propagating electromagnetic (EM) waves can be coupled into SSPPs efficiently. An important advantage of this approach is that the dispersion characteristics and the spatial confinement of SSPPs can be controlled simply by adjusting the geometrical parameters. Benefiting from this, SSPP couplers based on PGMs have been widely used in perfect absorbers,[16] miniaturized frequency selective surfaces,[17] ultra-thin cloaks,[18] etc. Nevertheless, limited by the long wavelength at low frequency in the microwave regime, the large size of metallic patterns for the unit-cell and thick dielectric substrates are inevitable to achieve high-efficiency control of the reflective phases. Heavy weight has seriously hindered practical applications of SSPP couplers at low frequencies. Hence, it is necessary to find a new and feasible design method to reduce both the dimensions and weights of SSPP couplers.

In this letter, we propose and design an ultra-thin and light-weight SSPP coupler based on the broadside coupled split ring resonators (BC-SRRs),[19,20] which consists of multilayer broadside coupled split ring resonators (SRRs) with strong capacitive couplings. According to the equivalent *L–C* circuit theory, the reflection phase can be precisely controlled and adjusted by varying the relevant geometric parameters of BC-SRRs. By designing a large phase gradient, an artificial parallel wave-vector can be obtained along the interface. Owing to the low occupation ratio and sub-wavelength dimensions of BC-SRRs, the coupler has a much lighter weight and low dielectric loss. As an example, a C-band SSPP coupler composed of BC-SRRs with $\lambda/12$ height is verified in this paper. We expect that the proposed method can provide an alternative to the designs of low-profile antennas, ultra-thin ab-

*Project supported by the National Natural Science Foundation of China (Grant Nos. 61331005, 61471388, and 61501503).

†Corresponding author. E-mail: wangjiafu1981@126.com

‡Corresponding author. E-mail: qushaobo@mail.xjtu.edu.cn

© 2018 Chinese Physical Society and IOP Publishing Ltd

sorbers, and other devices based on SSPPs.

2. Theoretical design and simulation

Split ring resonators (SRRs) are well-known subwavelength unit-cells for designing the PGMs. This kind of structure possesses both inductive and capacitive parts and behaves with the *LC* resonance-like property in response to incident EM waves.[21] To achieve a much smaller electrical size, the resonance frequency can be actually reduced by further increasing the effective capacitance or inductance. Mostly, in order to avoid enlarging the electrical size, the meander lines are usually adopted to obtain larger effective inductance, instead of straight lines. In a similar way, the coupling between neighboring metallic patterns can bring about considerable capacitive coupling to obtain larger effective capacitance. Single layer BC-SRR is a compact structure composed of two SRRs etched on either side of a dielectric substrate as illustrated in Fig. 1(a). Compared with the coplanar double-ring SRR, broadside coupling can produce an effective capacitance C_0, which is significantly larger than the split gap capacitances C_g and C_{metal}. The corresponding equivalent circuit model is given in Fig. 1(c). The total capacitance of the *L*–*C* circuit is dominated by the parallel capacitances between the two SRRs. The resonance frequency ω_1 is given by $\omega_1 = 1/\sqrt{L(C_g + C_{metal} + C_0)}$, where L is the total effective inductance. Due to the large capacitance resulting from broadside couplings, the resonance frequency of the BC-SRR is significantly reduced compared with that of the single SRR. Hence, if larger capacitive couplings are introduced into the unit-cell, the resonance frequency can be expected to be further reduced.

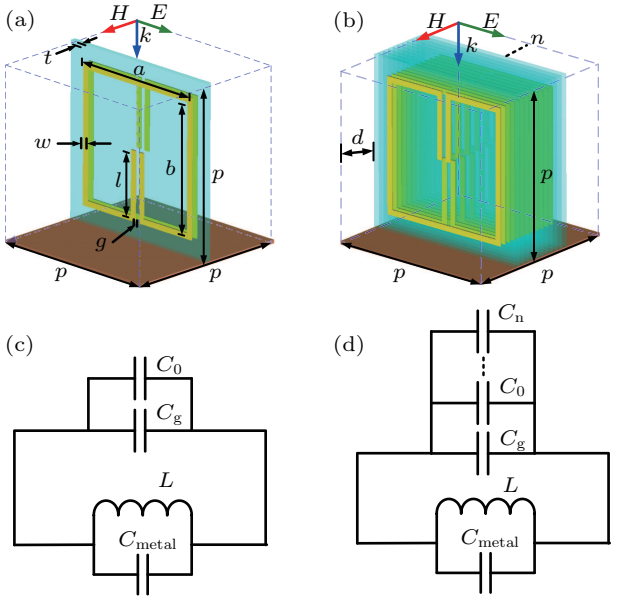


Fig. 1. (color online) BC-SRRs and equivalent circuits: (a) single layer BC-SRR, (b) multilayer BC-SRRs, (c) equivalent circuit for single BC-SRR, and (d) equivalent circuit for multilayer BC-SRRs.

Figure 1(b) illustrates the multi-layer BC-SRR composed of n SRRs with an alternate orientation of split gaps. The equivalent circuit of the multi-layer BC-SRR is shown in Fig. 1(d). Resonance frequency ω_{min} of the multilayer BC-SRR can be expressed as

$$\omega_{min} = 1/\sqrt{L[(C_1 + C_{metal} + (n-1)C_0]}. \quad (1)$$

Equation (1) shows that the resonance frequency will become lower as the number of SRR layers in a unit-cell is increased. Let the thickness of one BC-SRR layer be denoted as t, then the maximal layer number of SRR in a $p \times p \times p$ cubic lattice will be expressed as $n_{max} = p/t$. Therefore, the minimal resonance frequency is

$$\omega_{min} = 1/\sqrt{L[C_g + C_{metal} + (p/t - 1)C_0]}. \quad (2)$$

It can be found from Eq. (2) that for a given lattice constant p, we can reduce the resonance frequency by reducing the thickness t in order to accommodate more SRRs. Taking into account the air spacing d in a unit-cell, the maximal layer of SRRs can be further given by $n_{max} = (p-d)/t - 1$. Therefore, the minimal resonance frequency can be obtained from

$$\omega_{min} = 1/\sqrt{L\{C_g + C_{metal} + [((p-d)/t - 2)C_0]\}}. \quad (3)$$

Equation (3) is applicable to incidences with magnetic field lines threading through BC-SRRs. The broadside coupled capacitance C_0 between two adjacent SRRs can be approximately calculated by the capacitance formula of the flat plate capacitor, that is, $C_0 = \varepsilon_r w/t$, where ε_r is the dielectric constant of the substrate and w is the width of the metallic string line while the length per SRR is a constant. Then ω_{min} can be further expressed as

$$\omega_{min} = 1/\sqrt{L\{C_g + C_{metal} + [((p-d)/t - 2)(\varepsilon_r w/t)]\}}. \quad (4)$$

As indicated in Eq. (4), the resonance frequency is a function of the parameters of L, p, t, ε, and w. To demonstrate this theoretical model, we carry out a numerical simulation by using the frequency domain solver in the CST Microwave Studio. The metallic SRR patterns are etched on either side of the 0.25-mm-thick F4B substrate ($\varepsilon_r = 2.65$, $\tan\delta = 0.001$). Unit Cell boundaries are imposed along the $\boldsymbol{E}$ and $\boldsymbol{H}$ vector direction while Open Add Space boundaries are set to be along the propagation k direction. Figure 1(b) shows a BC-SRRs unit cell that consists of $n = 9$ BC-SRR layers in a 15 mm×15 mm×15 mm cubic lattice, while the relevant parameters are fixed at $a = b = 12$ mm, $l = 6$ mm, $w = g = 0.2$ mm. Figure 2(a) shows the plots of the reflection magnitude and phase under normal incidence versus frequency. It can be found that there is a sharp dip for S_{11} in the frequency interval of 196 MHz–211 MHz, where the about 300° abrupt phase change is produced. The center resonance

frequency is reduced down to 204 MHz, which means that the electrical dimensions are reduced to $\lambda/100 \times \lambda/100 \times \lambda/100$. In fact, by comparison with the scenario in Fig. 2(b), the center resonance frequency is shifted to a much lower frequency regime with the increase of the number n of BC-SRR layers. Simultaneously, the amplitudes of specular reflections generally decrease, which indicates that an increasing loss is caused by the BC-SRR resonance. The simulated results in Figs. 2(c) and 2(d) show that the trends of resonance frequency change with the strip-width w varying from 0.2 mm to 0.4 mm and the substrate thickness t varying from 0.25 mm to 0.5 mm, respectively. It should be noted that lower resonance frequency is obtained with the increase of w and the decrease of t.

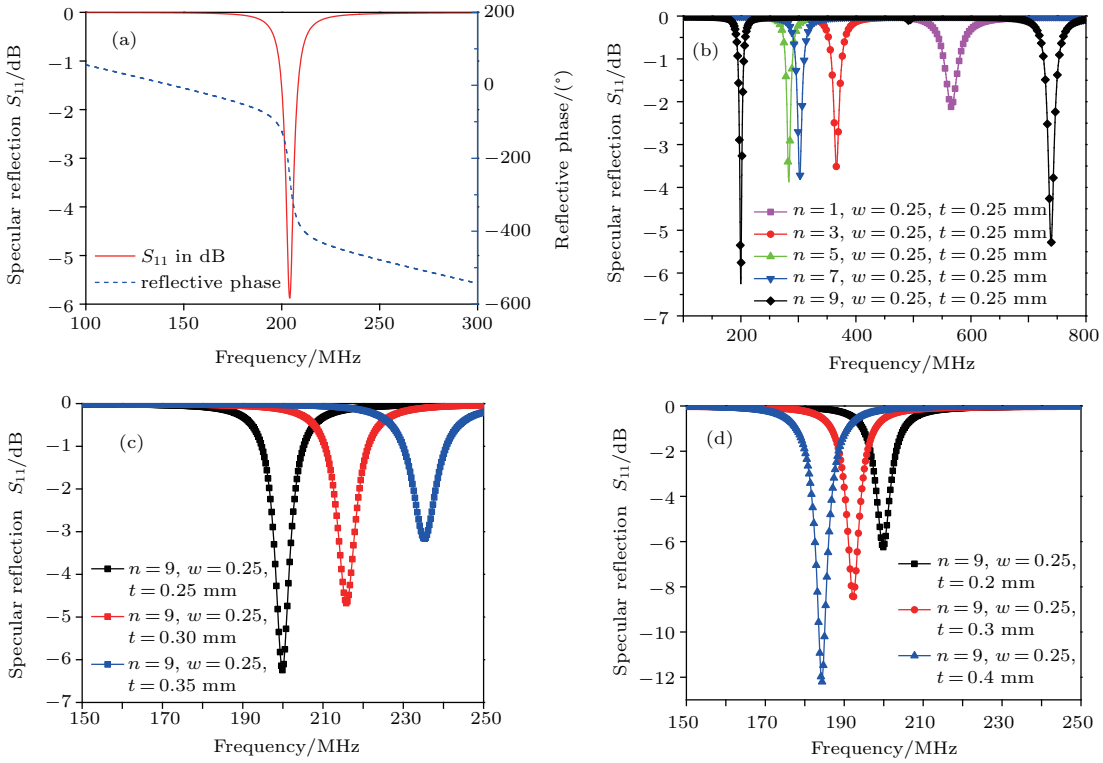


Fig. 2. (color online) (color online) Specular reflection properties of the unit-cell with $n = 9$ BC-SRR layers: (a) amplitude of S_{11} and reflection phase; (b), (c) and (d) frequency response of the amplitudes of S_{11} with different values of n, w, and t.

An additional wave vector ξ, as a well-studied method for PGM design, can be generated by periodically arranged metallic or dielectric resonators with $\Delta\Phi$ abrupt phase, where ξ is generally described as $\xi = \Delta\Phi/\Delta x$ for one-dimensional PGM. Under normal incidence, the x-component of reflective wave vector $k_x = \xi$ is larger than k in free space. Incident EM waves can be coupled as SSPP waves. Due to the deep-subwavelength size and low resonance frequency, multi-layer BC-SRRs can be a good candidate for designing the SSPP couplers. For minimizing the influence of the resonance loss and due to the limitation of machining precision and measured conditions, a single layer is adopted here to design the spoof SPP coupler working at 5.0 GHz. The unit cell includes a single BC-SRR layer, with $p = 5$ mm, $a = b = 3$ mm, and $w = g = 0.2$ mm. Metallic SRRs are etched on either side of a 0.5-mm-thick F4B dielectric substrate ($\varepsilon = 2.65$, $\tan\delta = 0.001$) and vertically placed on a 0.3-mm-thick metallized substrate. To produce an additional parallel wave vector ξ along the $-x$ direction, six sub-unit-cells are adopted to form a super-cell (as illustrated in Fig. 3(d)), with approximately a 60° phase change step. Each sub-unit-cell is composed of two identical BC-SRRs as shown in Fig. 3(a). The periodicity of the sub-unit-cell along the x direction is $\Delta x = 10.0$ mm. By precisely optimizing the length parameter l, we finally fix $l_1 = 0.24$ mm, $l_2 = 1.17$ mm, $l_3 = 1.45$ mm, $l_4 = 1.55$ mm, $l_5 = 1.66$ mm, and $l_6 = 2.15$ mm. The specular reflections S_{11} of six chosen unit cells are plotted in Fig. 3(b). It can be found that the averaged value is greater than -0.5 dB at 5.0 GHz, which means that an energy lower than 10% is lost by the resonance. As shown by the reflective phase distribution of six sub-unit-cells and the ratio of the phase gradient ξ to the wave vector k of free space in Fig. 3(c), for good impedance with the free space, the reflective phase gradient ξ is designed to be close to the wave vector of free space at 5.0 GHz, which is plotted with a red dot curve. To verify the properties of the SSPP coupler, a relevant simulation is conducted by using an infinitely large model through using the frequency-domain solver in CST Microwave Studio. Unit Cell boundaries are set to be along the $\boldsymbol{E}$ and $\boldsymbol{H}$ vector direction while "Open Add Space" boundaries are set to be along the propagation direction.

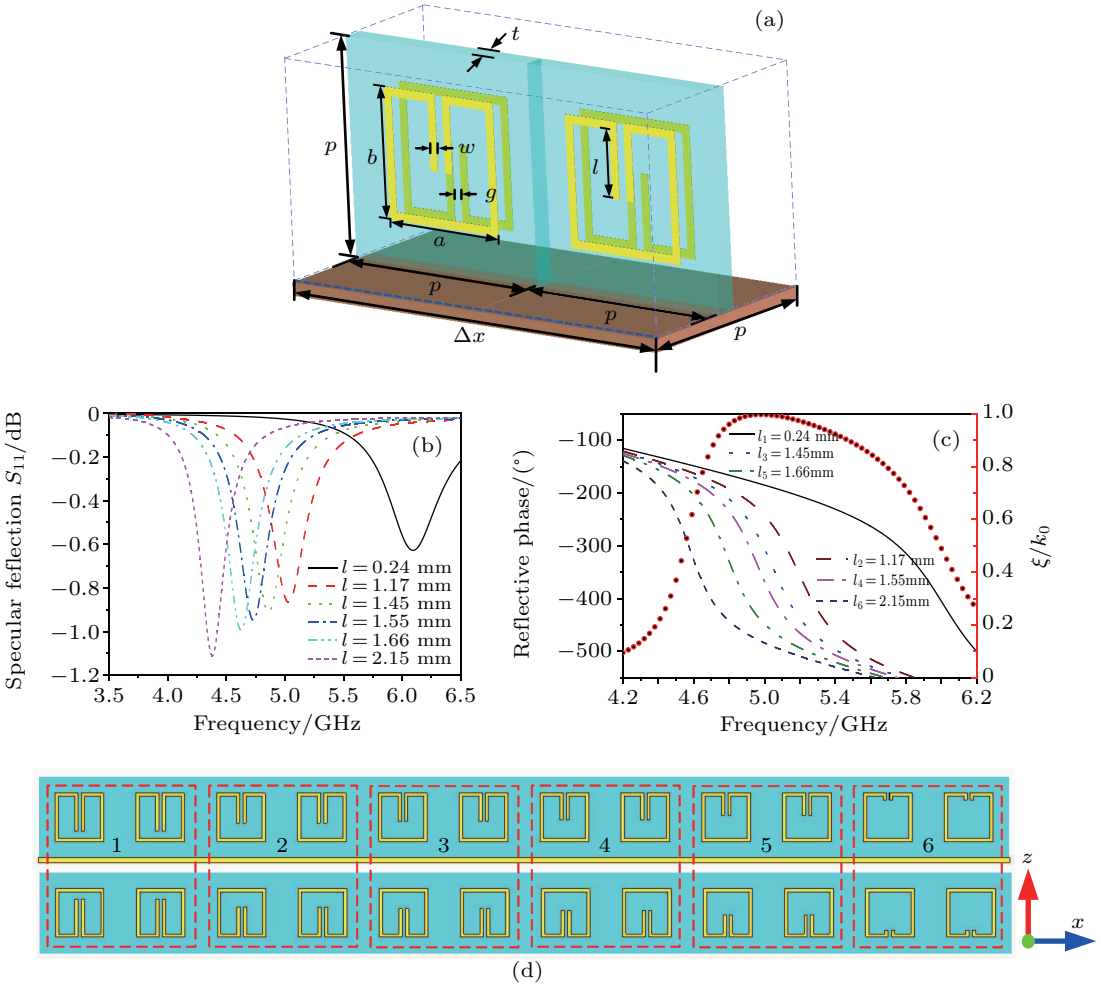


Fig. 3. (color online) (a) Perspective view of sub-unit-cell; ((b) and (c)) specular reflections S_{11}, reflective phase distributions of six sub-unit-cells and the ratio of the phase gradient ξ to the wave vector k of free space; (d) super-cell composed of six sub-unit-cells with $l = 0.24$ mm, 1.17 mm, 1.45 mm, 1.55 mm, 1.66 mm, and 2.15 mm, where the first and second layer present the front and back views, respectively.

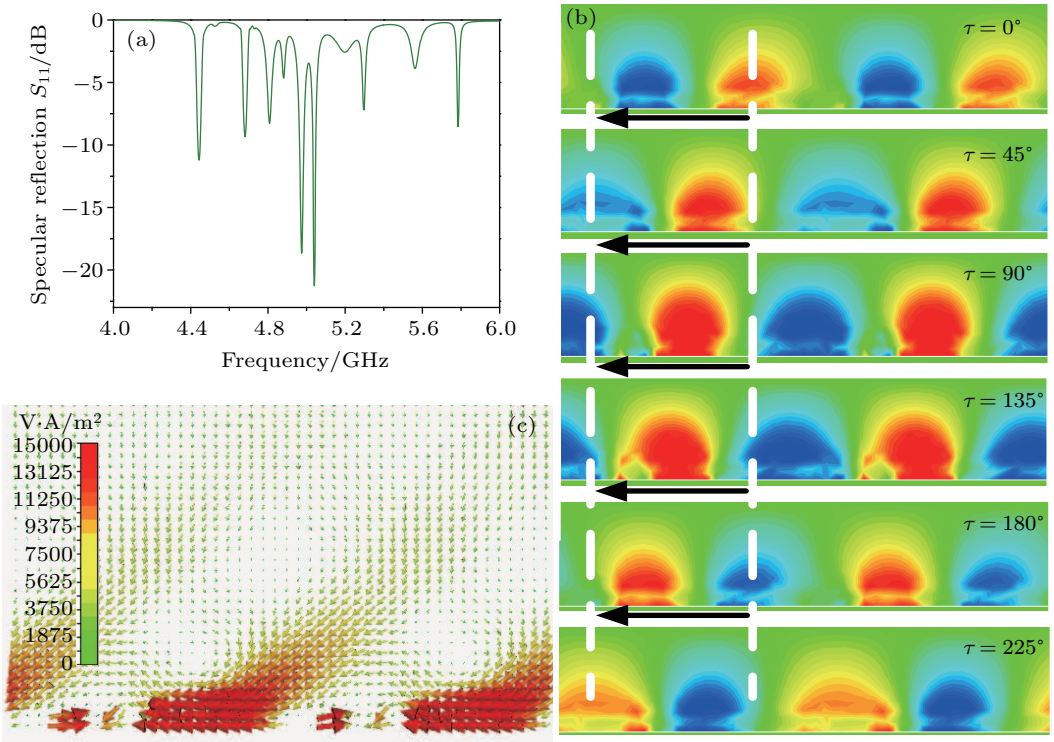


Fig. 4. (color online) (color online) Simulated results of the SSPP coupler at 5.05 GHz: (a) specular reflection S_{11} of the infinite coupler; (b) E_z field distributions at different phases as incident wave propagates; and (c) patterns of power flow.

To eliminate the influence of dielectric loss on the reflection property, a lossless F4B substrate and perfect electrical conductor are adopted to build the super-cell model. The specular reflection S_{11} under normal incidence is simulated and plotted in Fig. 4(a). The frequency response of the specular reflection S_{11} is drastically reduced down to -20.6 dB at 5.05 GHz.

In order to ascertain whether the low reflection results from SSPP coupling, E_z-field distribution and power flow are also monitored at 5.05 GHz. It can be seen that strongly-confined TM-SSPPs (the magnetic vector is always parallel to the coupler surface) are generated on the coupler as shown in Fig. 4(b). For clearer observation of the SSPPs, E_z-fields at different phases are also monitored. It is clear to see the E_z-fields move in the $-x$ direction along the surface when the τ value varies from 0° to 225°, where τ is defined as the phase of incident wave at the reference plane of the input port, which can also be understood as a time point in a periodic time. The coupled SSPP power also flows in the same direction as illustrated in Fig. 4(c). Within sub-wavelength dimensions, the EM energy is highly confined on the surface of the coupler, resulting in a strong field enhancement.

3. Experimental results

Considering the practical application of the SSPP coupler, a finite-size 300 mm $\times$300 mm (composed of 5×5 super-cells) prototype is fabricated by the printed circuit board technique as shown in Fig. 5(a). In the later process of fabrication, 0.5-mm-thick F4B substrate ($\varepsilon = 2.65$, $\tan\delta = 0.001$) slices are decorated with the BC-SRR patterns. Polymer foam bars ($\varepsilon_r \approx 1$) are inserted to keep the spacing between adjacent super-cells fixed, which is described in the inset of Fig. 5(a). The specular reflection spectrum in unit dB is first measured by using a pair of horn antennas. As plotted in Fig. 5(b), the reflection is significantly reduced down to -25 dB at 5.27 GHz. This indicates the high efficiency of the SSPP coupler. Due to the differences in the material electromagnetic parameter and fabrication error, the measured results each have a 0.2-GHz blue-shift compared with simulated ones. The second dip at 5.07 GHz and the third dip at 5.16 GHz are caused by other phase gradients achieved by the sub-unit-cells. Since the phase gradient is realized by a discrete quantity of sub-unit-cells, lower discretion would finally lead to lower coupling efficiency at the two dips than at the first dip. To further characterize the coupled SSPPs, E_z-field distributions on the x–o–z plane are measured by near-field scanning measurement at 5.07 GHz and 5.27 GHz, as shown in Figs. 5(c) and 5(d), respectively.

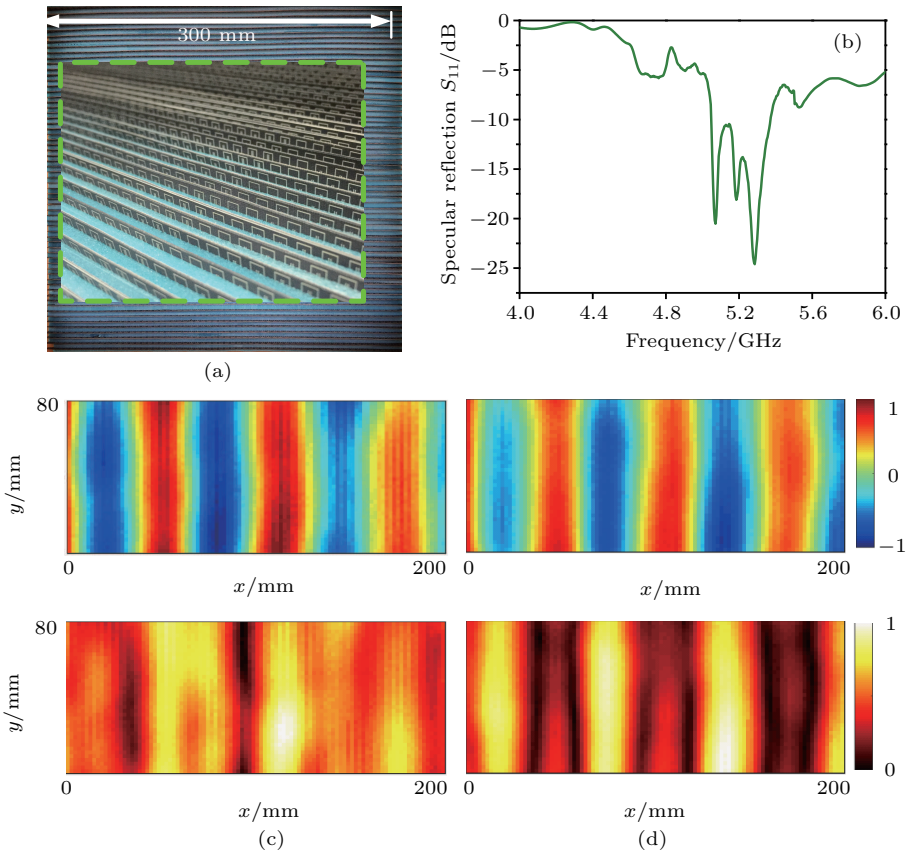


Fig. 5. (color online) (a) Photograph of SSPP coupler prototype; (b) measured specular reflection S_{11}; E_z-field distribution on the x–o–y plane of the coupler under normal x-polarized incident at (c) 5.07 GHz and (d) 5.27 GHz.

A distribution pattern composed of alternating fringes can be seen clearly. The dimensions of BC-SRR sub-unit-cells are only $1/12\lambda \times 1/12\lambda \times 1/12\lambda$, where λ is the wavelength at 5.27 GHz. A comprehensive comparison between our results with the results of the SSPP couplers presented in Refs. [22]–[24] is given in Table 1. The thickness t of the F4B substrate is a bit larger than that of the FR4 substrate. This is because of the smaller dielectric constant. However, the value of p_x and p_y of BC-SRR are comparatively reduced. Moreover, since the much lower occupation ratio, the proposed coupler possesses a much lower surface density, which is only $\rho \approx 0.98$ kg/m^2, even though the other listed work operates at a higher center frequency.

Table 1. Comprehensive comparison of our results with those from other similar studies.

References	Substrate material	Center frequency/GHz	Dimensions of unit cell p_x*p_y*t	Surface density /(kg/m^2)
[22]	FR4($\varepsilon_r = 4.3$, tanδ =0.025)	8	$0.9\lambda \times 0.13\lambda \times 0.03\lambda$	2.17
[23]	FR4($\varepsilon_r = 4.3$, tanδ =0.025)	15	$0.13\lambda \times 0.3\lambda \times 0.05\lambda$	2.17
[24]	F4B(($\varepsilon_r = 2.65$, tanδ =0.001))	10	$0.2\lambda \times 0.2\lambda \times 0.1\lambda$	5.91
This paper	F4B(($\varepsilon_r = 2.65$, tanδ =0.001))	5	$0.08\lambda \times 0.08\lambda \times 0.08\lambda$	0.98

4. Conclusions

In this work, we propose and design ultra-thin, light-weight SSPP couplers based on BC-SRRs. The resonance frequency of BC-SRRs could be significantly reduced by introducing large capacitive couplings of BC-SRRs within a sub-wavelength volume. As an example, a C-band SSPP coupler is realized by phase gradient BC-SRR arrays. Both the experimental results and simulation results verify the high efficiency and light weight of the SSPP coupler. With the characteristics of local field enhancement and deep-subwavelength confinement, such SSPP couplers have great potential applications in low-frequency devices, ultra-thin absorbers, advanced antenna design, radar imaging, etc.

References

[1] Maier S A 2007 *Plasmonics: Fundamentals and Applications* (New York: Springer-Verlag)

[2] Barnes W L, Dereux A and Ebbesen T W 2003 *Nature* **424** 824.

[3] Huidobro P A, Nesterov M L, Martin-Moreno L and García-Vidal F J 2010 *Nano Lett.* **10** 1985.

[4] Dai J, Dyakov S A and Yan M 2015 *Phys. Rev. B* **92** 035419

[5] Green R J, Frazier R A, Shakesheff K M, Davies M C, Roberts C J and Tendler S J 2000 *Biomaterials* **21** 1823

[6] Bozhevolnyi S I, Volkov V S, Devaux E, Laluet J Y and Ebbesen T W 2006 *Nature* **440** 508

[7] Fang N, Lee H, Sun C and Zhang X 2005 *Science* **308** 534

[8] Lin I T, Lai Y P, Fan C R and Liu J M 2015 *J. Selec.Top. Quantum Electron.* **22** 2

[9] Kajiwara S, Urade Y, Nakata Y, Nakanishi T and Kitano M 2016 *Phys. Rev. B* **93** 075126

[10] Yu N F, Genevet P, Kats M A, Aieta F, Tetienne J P, Capasso F and Gaburro Z 2011 *Science* **334** 333.

[11] Ni X J, Emani N K, Kildishev A V, Boltasseva A and Shalaev V M 2012 *Science* **335** 427

[12] Yu J B, Ma H, Wang J F, Li Y F, Feng M D and Qu S B 2015 *Chin. Phys. B* **24** 098102

[13] Li Y F, Zhang J Q, Qu S B, Wang J F, Zheng L, Zhou H, Xu Z and Zhang A X 2015 *Chin. Phys. B* **24** 014202

[14] Liu T J, Xi X, Ling Y H, Sun Y L, Li Z W and Huang L R 2015 *Acta Phys. Sin.* **64** 237802 (in Chinese)

[15] Fan Y, Qu S B, Wang J F, Zhang J Q, Feng M D and Zhang A X 2015 *Acta Phys. Sin.* **64** 184101 (in Chinese)

[16] Li P C, Zhao Y, Alu A and Yu E T 2011 *Appl. Phys. Lett.* **99** 221106

[17] Wang J F, Qu S B, Xu Z, Ma H, Wang X H, Huang D Q and Li Y F 2012 *Photon Nanostruct. Fundam. Appl.* **10** 540.

[18] Zhou J F, Koschny T, Zhang L, Tuttle G and Soukoulis C M 2006 *Appl. Phys. Lett.* **88** 221103

[19] Marqués R, Mesa F and Martel J 2003 *IEEE Trans. Anten. Propag.* **51** 2572.

[20] Wen Q Y, Zhang H W, Xie Y S, Yang Q and Liu Y L 2009 *Appl. Phys. Lett.* **95** 241111

[21] Costa F, Monorchio A and Manara G 2010 *IEEE Trans. Anten. Propag.* **58** 1551.

[22] Wang J F, Qu S B, Ma H, Xu Z and Zhang A X 2012 *Appl. Phys. Lett.* **101** 201104

[23] Sun S L, He Q, Xiao S Y, Xu Q, Li X and Zhou L 2012 *Nat. Mater.* **11** 426

[24] Chen H Y, Ma H, Wang J F, Qu S B, Li Y F, Wang J, Yan M B and Pang Y Q 2015 *Appl. Phys. A* **120** 287